PHYSICAL REVIEW B **93**, 165206 (2016)

Electron and chemical reservoir corrections for point-defect formation energies

Christoph Freysoldt, Björn Lange,* and Jörg Neugebauer
Max-Planck-Institut für Eisenforschung, Max-Planck-Straße 1, 40237 Düsseldorf, Germany

Qimin Yan,† John L. Lyons,‡ Anderson Janotti,§ and Chris G. Van de Walle
Materials Department, University of California Santa Barbara, California 93106-5050, USA
(Received 19 January 2016; published 22 April 2016)

Point-defect formation energies calculated within the framework of density functional theory often depend on the choice of the exchange and correlation (xc) functional. We show that variations between the local density approximation (LDA), generalized gradient approximation (GGA), and hybrid functionals mainly arise from differences in the position of the bulk valence-band maximum, as well as in the reference energies for the chemical potential obtained with distinct xc functionals. We demonstrate for point defects relevant for *p*-type GaN that these differences can be accounted for by corrections, reducing the maximum disagreement between the different functionals from more than 2 eV to below 0.2 eV. Our correction scheme should be useful for performing high-throughput calculations in cases where full hybrid functional calculations are prohibitively expensive.

DOI: 10.1103/PhysRevB.93.165206

I. INTRODUCTION

The calculation of defect formation energies by means of density functional theory (DFT) in a supercell geometry has evolved into a standard tool to address doping and doping limitations in semiconductor physics [1–3]. Calculated formation energies allow predicting, for example, equilibrium concentrations of intrinsic and extrinsic point defects or defect complexes. However, the predictive power of this approach appears limited: the calculated formation energy of point defects depends on details of the theoretical method, notably the exchange-correlation (xc) functional [4], and is also affected by spurious interactions between a defect and its periodic images in the supercell approach [5–8].

Traditional functionals such as the local density approximation (LDA) or the generalized gradient approximation (GGA) severely underestimate the band gaps of semiconductors and insulators. For a long time it was believed that this is mostly due to an insufficiently accurate description of unoccupied states, and hence correction schemes focused on the position of conduction bands (CBs) and defect states with CB-like character such as donors [9,10]. However, it became clear that also valence-band (VB) like states must be corrected [11], and that the relative position of the VB with respect to the averaged electrostatic potential is poorly described [12–14].

Hybrid functionals have emerged as a reliable approach for overcoming these problems. These functionals mix approximate (semi)local exchange functionals with exact nonlocal Hartree-Fock exchange, yielding excellent structural properties as well as quantitatively better band gaps and absolute band-edge positions [15,16]. Of course, hybrid functionals are also approximate and parameterized; how reliably a particular functional reproduces experiment is still under active research (see, for instance, Komsa and Pasquarello [17]). At present, however, hybrid functionals are the widely used choice to overcome the limitations of the conventional semilocal functionals. Unfortunately, hybrid functionals are computationally very demanding. This limits the size of affordable supercells, and makes scanning large numbers of possible defect configurations prohibitively time consuming. It therefore remains desirable to employ standard functionals to estimate the formation energy of candidate defects [18]. Such an approach is only effective, of course, if the calculations based on standard functionals are reliable in identifying the most relevant defects. In the present work, we propose such an approach.

We will compare the results of three widely used xc functionals: the LDA [19], the generalized gradient approximation of Perdew, Burke, and Ernzerhof (PBE) [20], and the screened hybrid functional of Heyd, Scuseria, and Ernzerhof (HSE) [21,22]. As a benchmark we consider magnesium-doped gallium nitride (GaN:Mg), which has a high technological relevance due to its use as the *p*-conductive layer in GaN-based light-emitting devices. Point defects in this material have been extensively studied both experimentally and theoretically [1,2,23–27]. For example, the study by Myers *et al.* [2] provides a detailed analysis of the energetics and electrical activity of various point defects in GaN:Mg at the level of PBE. The extensive set of defect structures investigated there will be used as a test set in the present study. Note that we use the term "defect" to include impurities, point defects, as well as complexes.

The defect formation energies obtained with the various xc functionals show an unacceptable scatter as discussed in Sec. III. We will analyze the origin of the differences in Sec. IV and show that they can be explained by an incomplete error cancellation between the calculations for defect supercells and the corresponding reference states. The incomplete cancellation of errors has been observed and addressed before, see, e.g., Refs. [4,28,29]. For instance, in their work on alumina Hine *et al.* [29] exploited the fact that the error cancellation between

*Present address: Department of Mechanical Engineering and Materials Science, Duke University, Durham, North Carolina 27708, USA.
†Present address: Molecular Foundry, Lawrence Berkeley National Laboratory, Berkeley, California 94720, USA.
‡Present address: Center for Functional Nanomaterials, Brookhaven National Laboratory, Upton, New York 11973, USA.
§Present address: Department of Materials Science and Engineering, University of Delaware, Newark, Delaware 19716-3106, USA.

solids (Al and Al_2O_3) works better than between solids and molecules (O_2). Building on this observation, they rewrote the oxygen reference energy in the defect-formation formalism described below in terms of the DFT total energies of Al and Al_2O_3 and the *experimental* formation enthalpy of Al_2O_3. Peng *et al.* [4] compared formation energies of GGA(+U) and HSE for defects in a range of oxides and nitrides. They proposed to apply corrections to the valence-band maximum (VBM) from GW calculations and to the atomic reference energies from a fit to a set of experimental compound formation enthalpies, thereby reducing the differences between the functionals to 0.34 eV on average. We will show here that by correcting the chemical potentials of the electrons and chemical elements for a specific system, the apparent differences between different functionals can be reduced to below 0.1 eV on average.

II. COMPUTATIONAL DETAILS

The key thermodynamic quantity for a point defect X in charge state q is its formation energy [1,3]

$$E^f[X^q] = E_{\text{tot}}[X^q] - E_{\text{tot}}[\text{bulk}] - \sum_i n_i \mu_i + q\mu_e + \Delta_q, \tag{1}$$

which depends on the chemical potentials μ_i of atoms that have been added ($n_i > 0$) or removed ($n_i < 0$) in order to construct the defect, and on the chemical potential for electrons μ_e. The total energy of the defect $E_{\text{tot}}[X^q]$ and the energy of the defect-free bulk reference $E_{\text{tot}}[\text{bulk}]$ are obtained by DFT. Δ_q is the finite-supercell size correction for charged defects [5,30], as explained below. For each functional, the internal coordinates of each cell are optimized using the bulk lattice constant for the employed functional.

We perform projector augmented wave (PAW) [31] calculations with the LDA [19], PBE, [20] or HSE [21,22] functionals, using the *Vienna Ab Initio Simulation Package* (VASP) [32,33] as well as the SPHInX package [34], and the VASP PAW potentials [33]. Most of the LDA and PBE calculations were done with the SPHInX package. We checked that both packages give the same results to within 0.05 eV. The Ga 3d electrons were treated as part of the frozen core. For HSE an exact-exchange mixing of $\alpha = 0.31$ and a screening of $\omega = 0.2\,\text{Å}^{-1}$ is used, which produces a band gap for wurtzite GaN of 3.46 eV. In our defect calculations we use an orthorhombic $3 \times 2 \times 2$ supercell, containing 96 atoms. For LDA and PBE, an energy cutoff of 476 eV and a $2 \times 2 \times 2$ Monkhorst-Pack mesh [35] ensure convergence for the total energy within 1 meV and the lattice constant within 0.01 Bohr. For HSE, the plane-wave cutoff was 300 eV. Relaxing the structure to the energetic minimum results in the bulk structural parameters in Table I. The lattice constants for LDA and HSE agree closely with experimental data, while PBE yields a slightly larger lattice constant. On the other hand, HSE reproduces the c/a ratio slightly worse (−0.2%) than LDA and PBE.

The chemical potentials μ_i represent the energies (in the implicit reference given by the DFT code) of the reservoirs that act as the sources of the individual species. The chemical potentials appear as parameters in Eq. (1), and can be chosen to correspond to specific physical growth scenarios. The chemical potentials are referenced to well-defined reference states [3], i.e.,

TABLE I. Structural parameters of wurtzite GaN obtained with different xc functionals and compared with experiment.

	LDA	PBE	HSE	exp[a]
a (Bohr)	6.04	6.14	6.06	6.0263
c/a	1.627	1.626	1.623	1.626
u	0.377	0.377	0.378	
gap (eV)	1.98	1.64	3.46	3.51

[a]Ref. [36]

$$\mu_i = \mu_i^0 + \Delta\mu_i, \tag{2}$$

where μ_i^0 is the (fixed) reference and $\Delta\mu_i$ is the value of the chemical potential for a specific scenario relative to the reference. The conventional standard reference state for each chemical element is the phase of that element at standard conditions, i.e., the bulk metals for Ga and Mg, and molecular N_2 and H_2 for nitrogen and hydrogen, respectively. Neglecting the effects of temperature and pressure, the reference energies are directly obtained from DFT total energies. For instance, μ_{Ga}^0 is given by

$$\mu_{\text{Ga}}^0 = \tfrac{1}{8} E^{\text{DFT}}(\text{Ga bulk}), \tag{3}$$

where $E^{\text{DFT}}(\text{Ga bulk})$ is the total energy of the eight-atom orthorhombic unit cell of Ga. Given these references, and assuming equilibrium with bulk GaN, we then obtain:

$$\Delta\mu_{\text{N}} + \Delta\mu_{\text{Ga}} = \Delta H^f(\text{GaN}), \tag{4}$$

where $\Delta H^f(\text{GaN})$ is the formation enthalpy of GaN. Both $\Delta\mu_{\text{N}}$ and $\Delta\mu_{\text{Ga}}$ can thus vary over a range given by the magnitude of the enthalpy of formation.

Similarly, the chemical potential of electrons μ_e is referenced to a standard reference, conventionally taken to be the VBM:

$$\mu_e = \varepsilon_{\text{VBM}} + \varepsilon_{\text{Fermi}}. \tag{5}$$

The VBM reference energy is likewise taken in the implicit reference of the DFT code used. The range of $\varepsilon_{\text{Fermi}}$ is typically taken to be the band gap, i.e., the Fermi energy can vary between the VBM and the conduction-band minimum (CBM).

As far as thermodynamics is concerned, chemical species and electrons can be treated on the same footing, and indeed, we will exploit this analogy in our discussions. To keep the distinction clear, however, we will generally restrict our use of the term "chemical potential" to refer to chemical species only, and use the term "Fermi energy" when discussing the chemical potential for electrons, thereby following the conventional terminology in the field of semiconductors.

The values of the chemical potential reference energies μ_i^0 and of the VBM energy ε_{VBM} are specific to a particular theoretical approach (xc functional, potentials, DFT code, etc.). The parameters $\Delta\mu_i$ and $\varepsilon_{\text{Fermi}}$, on the other hand, can be chosen to correspond to specific experimental conditions: In the case of the chemical potentials to reflect physical growth scenarios, and in the case of the Fermi level to represent specific electronic conditions (e.g., due to doping) in the material. In contrast to μ_i^0 and ε_{VBM}, the parameters $\Delta\mu_i$ and $\varepsilon_{\text{Fermi}}$ should be independent of the computational details.

For the purpose of listing defect formation energies, it is common practice not to use the "standard formation energies" ($\Delta\mu_i = 0$), but to employ a certain choice of limiting conditions, given by equilibrium with selected phases, and setting the Fermi energy to the VBM ($\varepsilon_{\text{Fermi}} = 0$). In our case, the reservoirs will be wurtzite GaN, orthorhombic Ga metal, hexagonal Mg metal, and the H_2 molecule, all at zero temperature. These choices correspond to $\Delta\mu_{\text{Ga}} = \Delta\mu_{\text{Mg}} = \Delta\mu_{\text{H}} = 0$ and, given Eq. (4), $\Delta\mu_{\text{N}} = \Delta H^f(\text{GaN})$. The corresponding values for the chemical potentials μ_i can then be directly extracted from DFT total energy calculations. For internal consistency, the energies of the reservoirs must be calculated at the same level of theory as the defect supercell and the perfect bulk system.

Formally, the choice of reservoirs for listing the defect formation energies is irrelevant. In practice, when one aims at comparing different theoretical approaches, or theory and experiment, the choice of the reservoirs used for comparison does matter (see, e.g., Hine *et al.* [29], Peng *et al.* [4]) since errors of a given xc functional in describing the defect, the perfect bulk, and the reservoirs of choice do not cancel out completely. We will discuss this in detail in Sec. IV B.

We will also examine charge-state transition levels, which are defined as

$$\varepsilon^{q_1/q_2} = \frac{E^f[X^{q_1}] - E^f[X^{q_2}]}{q_2 - q_1} - \varepsilon_{\text{VBM}} \,. \tag{6}$$

These correspond to the Fermi-level positions at which a defect changes its charge state. Note that these values do not depend on the chemical potentials.

Charged defect calculations in the supercell approach suffer from the long-range Coulomb interaction of the defect with its periodic images. The formation energy of a charged defect therefore depends on the chosen supercell size unless the interactions are corrected for [Δ_q in Eq. (1)] [5,30]. Finite-size errors can be a sizable effect that has the potential of changing the qualitative physics of the system. The case of the 3+ charge state of the nitrogen vacancy in GaN (V_N), calculated within LDA, is an excellent example. For commonly employed supercells consisting of approximately 100 atoms, V_N^{3+} is thermodynamically stable for Fermi levels in the lower part of the band gap, and the (3+/+) charge-state transition level appears in the band gap (see Table II). In the limit of infinite supercell size, however, V_N^{3+} is no longer stable, i.e., the (3+/+) level lies below the VBM [37] which in itself is a failure of LDA, as explained below. The charge corrections Δ_q recover the infinite-supercell-size limit at much smaller supercell sizes.

TABLE II. Charge-state transition levels for selected defects (in eV) with respect to the VBM, from Eq. (6), without supercell-size correction for charged defects. The defect-free supercell contains 96 atoms. Data from Ref. [2] (72 atoms) are listed for comparison.

defect	LDA	PBE	PBE[a]	HSE
$V_N^{3+/+}$	0.33	0.41	0.39	1.14
$(MgV_N)^{2+/0}$	0.35	0.40	0.45	1.17
$(MgHV_N)^{3+/+}$	0.36	0.43	0.33	1.21

[a]Ref. [2], 72-atom supercells, ultrasoft pseudopotentials (USPP).

III. APPLYING THE "STANDARD APPROACH"

The dominant defects in GaN:Mg as grown with metal-organic vapor phase epitaxy include substitutional Mg on the Ga site; interstitial hydrogen in the positive charge state, H^+, in the bond center (BC) or antibonding (AB) site; the nitrogen vacancy, V_N; and combinations of these point defects. In the following we use a similar notation as in Ref. [2], notably for the orientation of defects or defect complexes: Some defects can be viewed as modification of a Ga-N bond: H^+ inserted into (or attached to) a Ga-N bond, or a complex formed by Mg on a Ga site and a defect on a N site (V_N or H_N). For these defects, the orientation can be characterized by the two inequivalent types of Ga-N bonds: parallel to the *c*-axis (subscript $\parallel$), or one of the three Ga-N bonds lying largely in the *ab* plane (subscript $\perp$). For a detailed description of the defects we refer to Ref. [2] and references therein.

The calculated formation energies, based on the formalism described in Sec. II, are shown in Table III, where the rightmost three columns contain the differences between the

TABLE III. Defect formation energies calculated with LDA, PBE, and HSE, including the supercell-size correction of Ref. [5]. The chemical potentials correspond to equilibrium with bulk GaN, Ga, Mg, and the H_2 molecule (see text). The Fermi level is set to the VBM as calculated with each xc functional. All values in eV. The right columns show pairwise differences between the three functionals. The weighted rms error gives each of the eight defect classes equal weight.

	LDA	PBE	HSE	LDA − HSE	PBE − HSE	LDA − PBE
Mg^-	1.35	1.19	2.38	−1.03	−1.19	0.16
V_N^+	0.63	0.54	−0.18	0.81	0.72	0.09
V_N^{3+}	1.25	0.88	−1.13	2.38	2.01	0.37
$H^+_{\parallel\,(AB)}$	−0.07	0.16	−0.54	0.47	0.70	−0.23
$H^+_{\perp(AB)}$	−0.20	0.04	−0.69	0.49	0.73	−0.24
$H^+_{\parallel\,(BC)}$	−0.25	−0.11	−0.73	0.48	0.62	−0.14
$H^+_{\perp(BC)}$	−0.02	0.09	−0.52	0.50	0.61	−0.11
H_N^{2+}	−0.23	−0.12	−1.71	1.48	1.59	−0.11
$(MgH)^0_{\parallel(BC)}$	0.06	0.15	0.50	−0.44	−0.35	−0.09
$(MgH)^0_{\parallel(AB)}$	0.18	0.30	0.65	−0.47	−0.35	−0.12
$(MgH)^0_{\perp(AB\ Mg_\perp)}$	−0.03	0.12	0.41	−0.44	−0.29	−0.15
$(MgH)^0_{\perp(BC\ Mg_\perp)}$	0.30	0.38	0.69	−0.39	−0.31	−0.08
$(MgH)^0_{\perp(AB\ Ga_\parallel)}$	0.23	0.36	0.67	−0.44	−0.31	−0.13
$(MgH)^0_{\perp(AB\ Ga_\perp)}$	0.17	0.32	0.52	−0.35	−0.20	−0.15
$(MgV_N)^0_\parallel$	1.04	0.90	1.27	−0.23	−0.37	0.14
$(MgV_N)^0_\perp$	1.07	0.92	1.25	−0.18	−0.33	0.15
$(MgV_N)^{2+}_\parallel$	0.93	0.62	−0.42	1.35	1.04	0.31
$(MgV_N)^{2+}_\perp$	0.91	0.56	−0.44	1.35	1.00	0.35
$(MgH_N)^+_\parallel$	−0.23	−0.14	−0.78	0.55	0.64	−0.09
$(MgH_N)^+_\perp$	−0.27	−0.18	−0.74	0.47	0.56	−0.09
$(MgHV_N)^+_{\parallel\,(AB\ Mg)}$	0.16	0.29	−0.14	0.30	0.43	−0.13
$(MgHV_N)^{3+}_{\parallel\,(AB\ Mg)}$	0.61	0.56	−1.35	1.96	1.91	0.05
weighted rms error				1.12	1.10	0.18

TABLE IV. Charge-state transition levels of selected defects (in eV) with respect to the VBM, from Eq. (6), with supercell-size correction for charged defects.

Defect	LDA	PBE	HSE
$V_N^{3+/+}$	−0.31	−0.17	0.48
$(MgV)_N^{2+/0}$	0.06	0.14	0.85
$(MgHV)_N^{3+/+}$	−0.22	−0.14	0.61

three functionals. Different xc functionals clearly give rise to defect energies that can vary by a few eV (here up to 2.4 eV for V_N^{3+} in LDA vs. HSE). We have computed the root-mean-square (rms) deviation, giving equal weight to each of the eight defect classes. The weighted rms deviation compared to HSE is 1.12 eV for LDA and 1.10 eV for PBE, while LDA and PBE differ on average by 0.18 eV. These large errors between the semilocal functionals and HSE do not seem systematic—they vary in sign and magnitude from defect to defect. This suggests that any conclusions about the relative importance of the defects drawn at the level of LDA or PBE cannot be trusted.

Table IV lists the charge-state transition levels as defined in Eq. (6). As alluded to before, the (3+/+) V_N transition level is unstable at the LDA and PBE level of theory when charged supercell artifacts are corrected for, in accordance with previous findings for large supercells [37]. This is not the case for HSE, which is regarded as superior compared to LDA and GGA due to the vastly improved description of the band gap. Indeed, the higher relative position of deep charge-state transition levels in HSE and other hybrid functionals can be rationalized by a lowering of the VBM compared to LDA and GGA functionals [12–15,38].

Interestingly, the charge-state transition levels neglecting supercell-size corrections obtained with LDA and PBE (see Table II) agree with the HSE values including the supercell corrections much better (to within 0.5 eV) than what could have been estimated from the magnitude of the band gap error (up to 1.8 eV) and the charge corrections (up to 0.6 eV). It seems that earlier defect calculations (before HSE defect calculations and reliable charged defect corrections became practical about five years ago) have profited from a fortuitous error cancellation in some cases. Indeed, the charged-defect artifacts for typical supercells systematically decrease the spacing between charge-state transition levels [5], squeezing them into the too small band gap of LDA and PBE. This cancellation explains why the large number of defect calculations published in the 1990's and early 2000's (that were based on LDA/PBE and neglected supercell-size corrections) produced results that are often qualitatively correct and hence more relevant than could have been guessed by assessing the individual errors.

IV. CORRECTIONS TO REFERENCE ENERGIES

A. Electrons: VBM alignment

It has long been recognized that the errors in the valence- and conduction-band positions lead to errors in the defect formation energy as calculated in the standard approach that

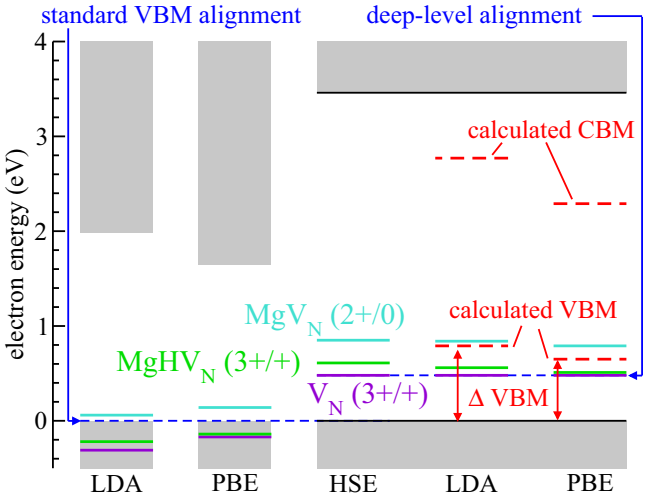

FIG. 1. Alignment of the electron chemical potential scales between LDA, PBE, and HSE. For each of the functionals, the VBM defines the energy zero. Left: the standard alignment, using the calculated VBM as a common point of reference for all defects. Right: modified alignment, using the (3+/+) charge-state transition level for V_N (violet lines) as the common point of reference. The charge-state transition levels (2+/0) for MgV_N (cyan) and (3+/+) for $MgHV_N$ (green) are also indicated, as well as the position of the calculated VBM and CBM of LDA and PBE.

can and should be corrected for [10,11]. Here, we take a slightly differently phrased, yet equivalent approach for deep defects. Instead of correcting the formation energy directly, we correct the position of the bulk valence band entering Eq. (1) as reference for the Fermi level [see Eq. (5)]. From a conceptual point of view, we thus correct for the known weakness of a functional in describing the extended host states, while leaving the description of the localized defect states unaltered. This is appropriate for defects that possess well-localized defect states within the band gap.

In order to obtain values for the valence-band shift, we will use the HSE data as the "best available theory" reference. We thus need the relative position of the LDA or PBE valence-band edges with respect to HSE. Such alignments have been discussed in the literature and can be based on the position of the average electrostatic potential [39] or on the alignment of the vacuum level [38]. Recent studies indicate that localized defect states in the band gap suffer less from the band-gap problem if referenced to the average electrostatic potential [13]. In the spirit of the Langer-Heinrich rule [40] and the *marker method* [41], we align the energy scales via the charge-state transition level of a deep and spatially well localized defect, specifically the $V_N^{3+/+}$ transition level. This is achieved by shifting the VBM of LDA down by −0.785 eV and that of PBE by −0.645 eV, as shown schematically in Fig. 1. These shifts agree with alternative schemes (electrostatic potential, vacuum level) to within ∼ 0.3 eV. Note that the VBM and the conduction-band minimum (CBM) as calculated from the respective functional are then no longer needed (see Fig. 1).

Applying the above alignment substantially reduces the differences between the LDA, PBE, and HSE formation energies for charged defects. The charge-state transition levels

TABLE V. Charge-state transition levels after applying corrections $\Delta\varepsilon_{\mathrm{VBM}}$ to the position of the VBM of LDA and PBE. The corrections have been chosen to bring the $V_N^{3+/+}$ into agreement with HSE, which are therefore marked with "!".

Defect	LDA	PBE	HSE
$V_N^{3+/+}$	0.48!	0.48!	0.48
$MgV_N^{2+/0}$	0.84	0.79	0.85
$MgHV_N^{3+/+}$	0.56	0.51	0.61
$\Delta\varepsilon_{\mathrm{VBM}}$	−0.79	−0.65	0

(Table V) agree to within 0.1 eV. The improvement for the transition levels is not too surprising, since the transition levels of Table V all derive from the $V_N^{3+/+}$ transition level. Yet, the formation energies listed in Table VI and visualized in Fig. 2

TABLE VI. Defect formation energies calculated with LDA, PBE, and HSE, including supercell-size corrections [5], and with a correction applied by shifting the VBM: The VBM values of LDA and PBE (used for referencing the Fermi level) have been adjusted as indicated in the first row of the Table to bring the $V_N^{3+/+}$ level in agreement with HSE (see text and Table V). All values in eV. The right columns show pairwise differences between the three functionals. The weighted rms error gives each of the eight defect classes equal weight.

	LDA	PBE	HSE	LDA − HSE	PBE − HSE	LDA − PBE
$\Delta\varepsilon_{\mathrm{VBM}}$	−0.79	−0.65				
Mg^-	2.14	1.84	2.38	−0.25	−0.55	0.30
V_N^+	−0.16	−0.11	−0.18	0.02	0.08	−0.05
V_N^{3+}	−1.11	−1.06	−1.13	0.02	0.07	−0.05
$H^+_{\parallel\,(AB)}$	−0.86	−0.49	−0.54	−0.32	0.06	−0.37
$H^+_{\perp(AB)}$	−0.99	−0.61	−0.69	−0.30	0.09	−0.38
$H^+_{\parallel\,(BC)}$	−1.04	−0.76	−0.73	−0.31	−0.03	−0.28
$H^+_{\perp(BC)}$	−0.81	−0.56	−0.52	−0.29	−0.04	−0.25
H_N^{2+}	−1.80	−1.41	−1.71	−0.09	0.30	−0.39
$(MgH)^0_{\parallel(BC)}$	0.06	0.15	0.50	−0.44	−0.35	−0.09
$(MgH)^0_{\parallel(AB)}$	0.18	0.30	0.65	−0.47	−0.35	−0.12
$(MgH)^0_{\perp(AB\ Mg_\perp)}$	−0.03	0.12	0.41	−0.44	−0.29	−0.15
$(MgH)^0_{\perp(BC\ Mg_\perp)}$	0.30	0.38	0.69	−0.39	−0.31	−0.08
$(MgH)^0_{\perp(AB\ Ga_\parallel)}$	0.23	0.36	0.67	−0.44	−0.31	−0.13
$(MgH)^0_{\perp(AB\ Ga_\perp)}$	0.17	0.32	0.52	−0.35	−0.20	−0.15
$(MgV_N)^0_\parallel$	1.04	0.90	1.27	−0.23	−0.37	0.14
$(MgV_N)^0_\perp$	1.07	0.92	1.25	−0.18	−0.33	0.15
$(MgV_N)^{2+}_\parallel$	−0.64	−0.67	−0.42	−0.22	−0.25	0.03
$(MgV_N)^{2+}_\perp$	−0.66	−0.73	−0.44	−0.22	−0.29	0.07
$(MgH_N)^+_\parallel$	−1.02	−0.79	−0.78	−0.24	−0.01	−0.23
$(MgH_N)^+_\perp$	−1.06	−0.83	−0.74	−0.32	−0.08	−0.23
$(MgHV_N)^+_{\parallel\,(AB\ Mg)}$	−0.63	−0.36	−0.14	−0.49	−0.22	−0.27
$(MgHV_N)^{3+}_{\parallel\,(AB\ Mg)}$	−1.75	−1.38	−1.35	−0.40	−0.02	−0.37
weighted rms error				0.29	0.28	0.26

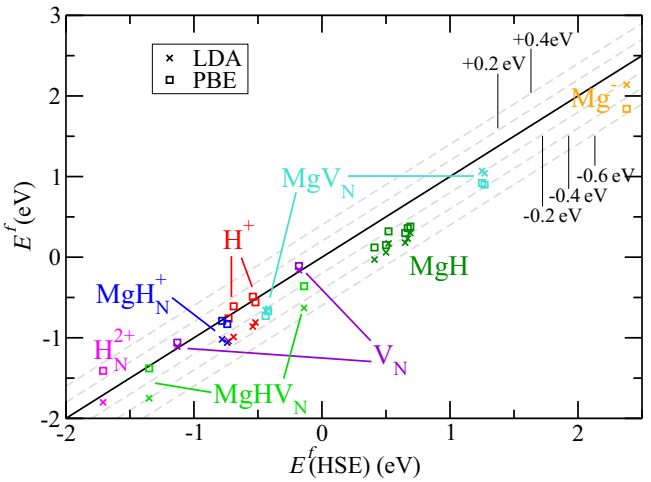

FIG. 2. Comparison of the formation energies of LDA (crosses) and PBE (squares) with those of HSE, with corrections for the VBM (see Table VI). Perfect agreement corresponds to the solid line. Dashed lines delimit deviations within the indicated bounds.

compare much better to each other even for defects completely unrelated to V_N. The maximum error is reduced to 0.55 eV (PBE vs HSE for Mg^-). A close inspection of Table VI and Fig. 2 shows that the error is now dominated by systematic shifts for the individual defect classes.

Figure 3 depicts the main principle of the VBM alignment with the help of plots of formation energy (E^f) vs Fermi level ($\varepsilon_{\mathrm{Fermi}}$) for LDA, PBE, and HSE. More precisely, we first note that the formation energy [Eq. (1)] depends on the absolute electron chemical potential $\mu_e = \varepsilon_{\mathrm{VBM}} + \varepsilon_{\mathrm{Fermi}}$ [Eq. (5)] in the implicit reference of the respective DFT bulk calculation. We then attach two Fermi energy scales to this plot: The bottom scale in each graph corresponds to the standard scheme, where the Fermi energy $\varepsilon_{\mathrm{Fermi}} = \mu_e - \varepsilon_{\mathrm{VBM}}$ relative to the VBM at the respective level of theory is indicated. The top scale for LDA and PBE corresponds to the adjusted VBM. The three graphs in Fig. 3 show the same range of the adapted scale. The gray part marks the bulk valence band within LDA and PBE, respectively. The formation energies of the standard scheme, listed in Table III, correspond to the crossing points of the formation energy lines with the $\mu_e = \varepsilon_{\mathrm{VBM(DFT)}}$ vertical line. It is obvious that errors in correctly positioning the VBM related to the choice of the xc functional have a direct and large impact on the formation energy of charged defects. The formation energies in the adjusted VBM scheme, listed in Table VI, correspond to the crossing points with the adjusted VBM at the left edge of the graph (no adjustment for HSE). Inspection of Fig. 3 drives home the point that the energies of the various defects are much more consistent with each other than the cut at the calculated (functional-specific) VBM suggests.

B. Reference energies for chemical elements

Despite the improvements resulting from the alignment of the VBM, systematic differences remain in the formation energies of Table VI and Fig. 2. For instance, the formation energies of all Mg-containing defects are lower in LDA by

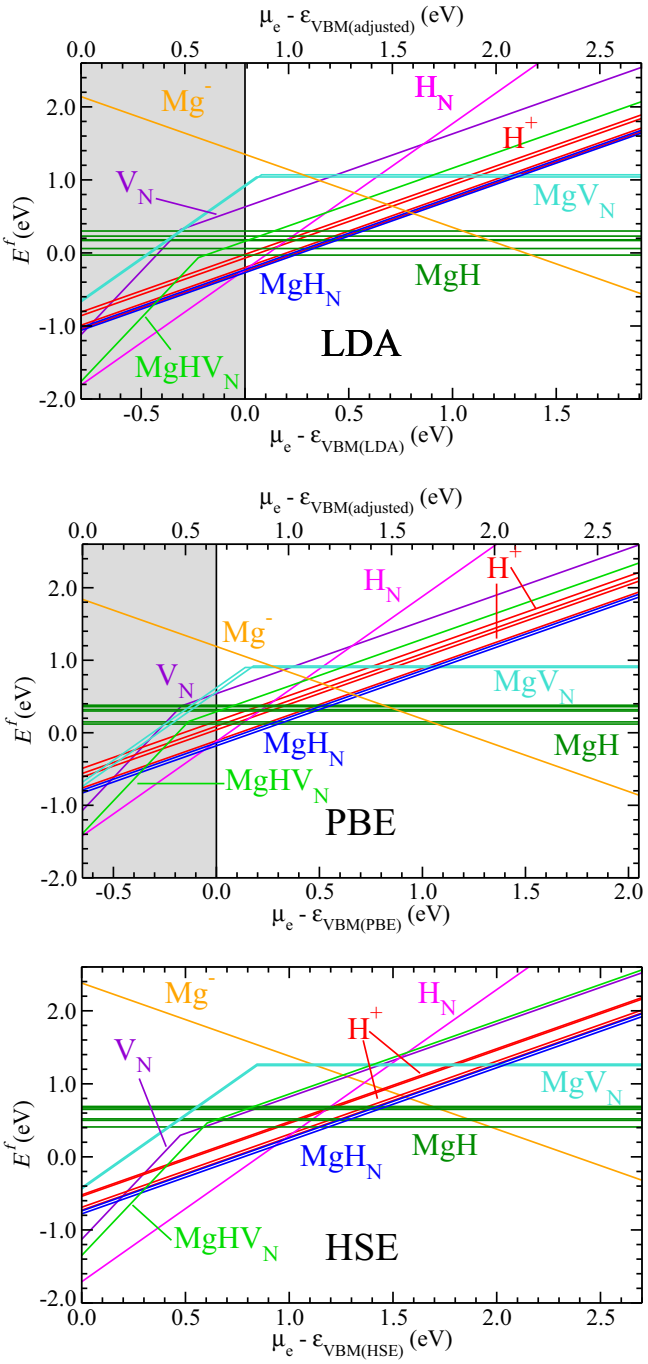

FIG. 3. Defect formation energies as a function of electron chemical potential $\mu_e = \varepsilon_{\mathrm{VBM}} + \varepsilon_{\mathrm{Fermi}}$, calculated with LDA, PBE, and HSE. The bottom scale reflects the standard referencing scheme with respect to the calculated VBM at the respective level of theory. The top scale for LDA and PBE reflects the adjusted scale.

0.2–0.5 eV compared to HSE. Similarly, the protonlike H^+ defects are too low by 0.3 eV. Such systematic deviations arise from the incomplete error cancellation of the underlying DFT calculations, namely the defect-containing supercell, the perfect bulk cell, and the various reference systems (Mg and Ga metal, and H_2).

In analogy to the approach taken for the VBM as reference state for the electron chemical potential, we will adjust the reference energies μ_i^0, entering Eq. (1) via Eq. (2), to account for the differences in the description of the employed reservoirs by different functionals, as previously proposed by Peng *et al.* [4].

To be specific, let us develop the analogy for the case of the nitrogen reference energy, μ_{N}^0. The standard reference state is the nitrogen molecule N_2 at zero temperature and the reference energy (in the implicit reference of the DFT code used) is

$$\mu_{\mathrm{N}}^0(\mathrm{N_2}) = \tfrac{1}{2} E^{\mathrm{DFT}}(\mathrm{N_2}). \tag{7}$$

It is well known that the errors in the total energy from a specific xc functional do not cancel out between molecules and solids [4,28,29,42]. It is here where the choice of the reservoirs for the comparison of defect energies and the consistent use of the same level of theory comes into play. For instance, let us assume equilibrium with bulk GaN [see Eq. (4)] and Ga-rich conditions, i.e., equilibrium with bulk Ga ($\Delta\mu_{\mathrm{Ga}} = 0$). In this scenario—which we will abbreviate with GaN/Ga—the nitrogen chemical potential is given by

$$\Delta\mu_{\mathrm{N}}(\mathrm{GaN/Ga}) = \Delta H^f(\mathrm{GaN}). \tag{8}$$

If $\Delta H^f(\mathrm{GaN})$ is calculated consistently at the level of theory used for the defects as

$$\Delta H^f(\mathrm{GaN}) = E^{\mathrm{DFT}}(\mathrm{GaN}) - \mu_{\mathrm{Ga}}^0 - \mu_{\mathrm{N}}^0, \tag{9}$$

the absolute nitrogen chemical potential for Eq. (1) becomes

$$\mu_{\mathrm{N}}(\mathrm{GaN/Ga}) = \mu_{\mathrm{N}}^0 + \Delta\mu_{\mathrm{N}} = E^{\mathrm{DFT}}(\mathrm{GaN}) - \mu_{\mathrm{Ga}}^0 \tag{10}$$

and hence independent of the molecular reference.

In experiment, chemical potentials are usually limited to the stability region of the host material

$$\Delta\mu_{\mathrm{N}}(\mathrm{GaN/Ga}) \leqslant \Delta\mu_{\mathrm{N}} \leqslant 0, \tag{11}$$

very much like the Fermi energy is limited to the band gap

$$\mathrm{VBM} \leqslant \varepsilon_{\mathrm{Fermi}} \leqslant \mathrm{CBM}. \tag{12}$$

It is therefore natural to use one of the two limits for the comparison of defect energies. Which of the two limits is used (GaN/Ga or N_2) is formally arbitrary. In practice, with the use of imperfect functionals, the choice of the reference state does matter, in particular if the formation enthalpy of the host material is not well reproduced. This can be seen as the analog of the band-gap problem.

Indeed, choosing a computational reservoir in order to optimize the error cancellation between the host compound and the reservoirs has been exploited before, e.g., by Finnis *et al.* [29,42] for Al_2O_3 in contact with oxygen gas. The computational reservoirs for the DFT calculations were Al_2O_3 and bulk Al, thereby eliminating the need to calculate the notoriously problematic O_2 molecule. The oxygen reference energy was then obtained from

$$\Delta H^f(\mathrm{Al_2O_3}) = E^{\mathrm{DFT}}(\mathrm{Al_2O_3}) - 2\mu_{\mathrm{Al}}^0 - 3\mu_{\mathrm{O}}^0 \tag{13}$$

using the *experimental* formation enthalpy of Al_2O_3.

Let us invoke the analogy with the Fermi energy again. Replacing the calculated formation enthalpy of GaN by the correct one and keeping the calculated Ga reference energy

unchanged corresponds to correcting the band gap and keeping the VBM unchanged. Yet, as we have seen above for the case of the electrons, corrections must be applied in general to *both* limits, the VBM and CBM. Analogously, we should apply a correction $\Delta\mu^0$ to both the N and Ga reference energies. Note that these reference energy corrections $\Delta\mu^0$ are independent of the chemical-potential scenario expressed by a specific choice of $\Delta\mu$.

We will again use the HSE results for defining corrections to the LDA and PBE reference energies. HSE generally reproduces thermochemical data rather well. The experimental formation enthalpy of GaN has been debated [43–45], and extrapolations from high-temperature experiments to standard conditions range between −1.15 eV and −1.71 eV [45]. Both LDA (−1.50 eV) and HSE (−1.34 eV) values fall in this range, while PBE yields a smaller value (−0.90 eV).

For Ga and N, we require that the corrections reproduce the HSE enthalpy of formation, i.e.,

$$E^{\mathrm{DFT}}(\mathrm{GaN}) - E^{\mathrm{DFT}}(\mathrm{Ga}) - \tfrac{1}{2}E^{\mathrm{DFT}}(\mathrm{N_2}) - \Delta\mu_{\mathrm{Ga}}^{0,\mathrm{DFT}} - \Delta\mu_{\mathrm{N}}^{0,\mathrm{DFT}} = \Delta H^{f,\mathrm{HSE}}(\mathrm{GaN}), \quad (14)$$

where the superscript DFT stands for either LDA or PBE. This leaves one free parameter to be determined, which then makes the defect energies consistent over the entire chemical-potential range. For the impurity elements Mg and H, no lower limit exists.

In practice, we proceed as follows: first, we set the correction of the Ga reference energy, which defines the nitrogen reference energy via Eq. (14), to bring the formation energy of the nitrogen vacancy in agreement with HSE. This is achieved by $\Delta\mu_{\mathrm{Ga}}^0 = +0.025$ eV for LDA, and +0.075 eV for PBE. The corresponding corrections for nitrogen [cf. Eq. 14] are $\Delta\mu_{\mathrm{N}}^0$=+0.19 eV for LDA and +0.68 eV for PBE, respectively. The value for the correction to the H chemical potential is a compromise between the protonlike H^+ and substitutional H_{N}^{2+} defects, amounting to −0.2 eV and +0.15 eV for LDA and PBE, respectively. Last, the correction to the Mg reference energy is set to −0.2 eV (LDA) and −0.3 eV (PBE) in order to reduce the overall disagreement of Mg-containing defects.

The resulting corrected formation energies as well as the differences between the different functionals are collected in Table VII and visualized in Fig. 4. It is obvious that the corrections to the reference energies lead to a further improvement of the agreement between the different functionals. The root-mean-square errors are 0.1 eV or less, and the maximum errors are all below 0.2 eV. We note that these errors are of the same order as the uncertainties inherent in the potential alignment for the supercell charge corrections (∼0.05 eV) or the effect of implementational details between the VASP and SPHInX codes (∼0.05 eV). We further note that adapting a lattice constant different from the optimized lattice constant for each functional, and hence putting the supercells under compressive or tensile stress, changes the defect formation energies considerably and proportional to the defect excess volume. The agreement between different functionals becomes worse if the lattice constant is forced to be the same.

TABLE VII. Defect formation energies calculated with LDA, PBE, and HSE, including supercell-size corrections [5] and a correction applied by shifting the VBM, as in Table VI. In addition, the reference energies of LDA and PBE have been adjusted as indicated at the top of the table. The energies of V_{N} have been used to adjust μ_{Ga}^0; the differences are zero by construction and are marked =0!. All values in eV. The right columns show pairwise differences between the three functionals. The weighted rms error gives each of the eight defect classes equal weight.

	LDA	PBE	HSE	LDA − HSE	PBE − HSE	LDA − PBE
$\Delta\varepsilon_{\mathrm{VBM}}$	−0.79	−0.65				
$\Delta\mu_{\mathrm{Mg}}^0$	−0.20	−0.30				
$\Delta\mu_{\mathrm{Ga}}^0$	+0.03	+0.08				
$\Delta\mu_{\mathrm{H}}^0$	−0.20	+0.15				
Mg^-	2.36	2.21	2.38	−0.02	−0.17	0.15
V_{N}^+	−0.18	−0.18	−0.18	=0!	=0!	=0!
V_{N}^{3+}	−1.13	−1.13	−1.13	=0!	=0!	=0!
$H_{\parallel\,(\mathrm{AB})}^+$	−0.66	−0.64	−0.54	−0.12	−0.09	−0.02
$H_{\perp(\mathrm{AB})}^+$	−0.79	−0.76	−0.69	−0.09	−0.06	−0.03
$H_{\parallel\,(\mathrm{BC})}^+$	−0.84	−0.91	−0.73	−0.11	−0.18	0.07
$H_{\perp(\mathrm{BC})}^+$	−0.61	−0.71	−0.52	−0.08	−0.19	0.10
H_{N}^{2+}	−1.63	−1.64	−1.71	0.08	0.07	0.01
$(\mathrm{MgH})_{\parallel(\mathrm{BC})}^0$	0.49	0.38	0.50	−0.01	−0.13	0.11
$(\mathrm{MgH})_{\parallel(\mathrm{AB})}^0$	0.61	0.53	0.65	−0.05	−0.13	0.08
$(\mathrm{MgH})_{\perp(\mathrm{AB\ Mg}_\perp)}^0$	0.40	0.35	0.41	−0.02	−0.06	0.05
$(\mathrm{MgH})_{\perp(\mathrm{BC\ Mg}_\perp)}^0$	0.73	0.61	0.69	0.04	−0.09	0.12
$(\mathrm{MgH})_{\perp(\mathrm{AB\ Ga}_\parallel)}^0$	0.66	0.59	0.67	−0.02	−0.09	0.07
$(\mathrm{MgH})_{\perp(\mathrm{AB\ Ga}_\perp)}^0$	0.60	0.55	0.52	0.07	0.03	0.05
$(\mathrm{MgV_N})_\parallel^0$	1.24	1.20	1.27	−0.03	−0.07	0.04
$(\mathrm{MgV_N})_\perp^0$	1.27	1.22	1.25	0.02	−0.03	0.05
$(\mathrm{MgV_N})_\parallel^{2+}$	−0.44	−0.37	−0.42	−0.02	0.05	−0.07
$(\mathrm{MgV_N})_\perp^{2+}$	−0.46	−0.43	−0.44	−0.02	0.01	−0.03
$(\mathrm{MgH_N})_\parallel^+$	−0.62	−0.64	−0.78	0.17	0.15	0.02
$(\mathrm{MgH_N})_\perp^+$	−0.66	−0.68	−0.74	0.08	0.07	0.02
$(\mathrm{MgHV_N})_{\parallel\,(\mathrm{AB\ Mg})}^+$	−0.23	−0.21	−0.14	−0.09	−0.07	−0.02
$(\mathrm{MgHV_N})_{\parallel\,(\mathrm{AB\ Mg})}^{3+}$	−1.35	−1.23	−1.35	0.01	0.13	−0.12
weighted rms error				0.07	0.10	0.07

C. Discussion

Our results clearly indicate that differences in the reference energies for electrons (the VBM) and chemical elements account for a very significant part of the differences in the formation energies calculated in the standard approach. As Table VII shows, our approach for adjusting the reference energies brings the LDA and PBE results in close agreement with the HSE results. This suggests that LDA and PBE may serve as reliable approaches to pre-screen a large set of defect configuration candidates. Of course, we have purposely selected defects that are *qualitatively* correctly described at the level of LDA or PBE. Failures must be expected when

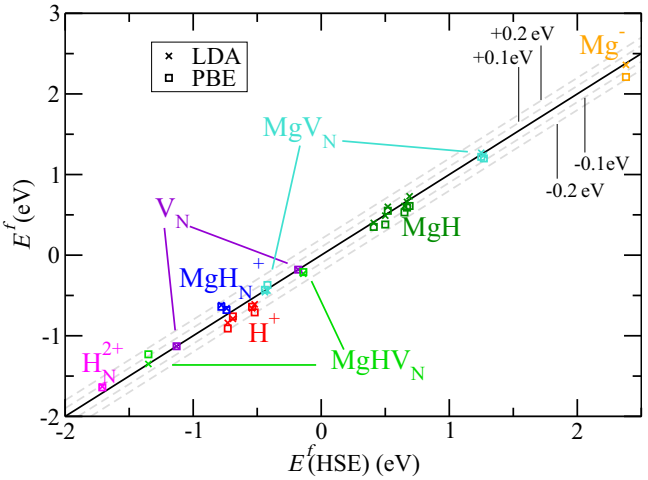

FIG. 4. Comparison of the formation energies of LDA (crosses) and PBE (squares) with those of HSE, with corrections for the VBM and for the energies of the reference systems (see Table VII). Perfect agreement corresponds to the solid line. Dashed lines delimit deviations within the indicated bounds.

electron (or hole) localization become important [46–48], or when defect states that are actually deep levels in the gap are hidden by the band edges—even though [as we saw in the case of the $(3+/+)$ level of V_N], charged-supercell artifacts (if not properly corrected) may apparently shift them into the LDA or PBE band gap in some cases, fortuitously helping to identify and study such levels. We note in passing that Sadigh *et al.* have recently proposed a scheme to describe bulk polarons even at the level of semilocal functionals [49]; whether it works also for polaronic effects in defects remains to be investigated.

The corrections to the chemical potentials also help to identify more clearly where LDA, PBE, and HSE show significant differences. For instance, LDA and PBE systematically place protonlike H defects lower than HSE compared to H_N. This may be due to a reduction of the artificial self-energy within the substitutional hydrogen atom from the exact-exchange part of HSE. We believe that the described correction scheme may also help to assess the performance of advanced theoretical methods in separating the improvement of the description of individual defects from the changes in the description of the reference systems.

Finally, we note that in our work, the corrections to the chemical potentials are derived by comparison to HSE calculations. In general, however, experimental or high-level theoretical data for selected cases might be used to define appropriate corrections.

V. SUMMARY & CONCLUSION

We have calculated formation energies of important point defects in GaN:Mg using LDA, PBE, and HSE. The standard approach, using each functional consistently to calculate the energies of the perfect bulk, the defect supercells and the relevant reference states of chemical elements shows differences of up to 2.4 eV between the different functionals. We show that these differences largely arise from the incomplete error cancellation when comparing different materials within the same functional, in addition to the well-known weakness of LDA and PBE to reproduce band-edge positions of semiconductors or insulators. By correcting for known failures in the reference chemical potentials of the electron (in other words: the valence-band maximum) and of the chemical elements in an analogous way, we arrive at a consistent picture: After corrections are applied, the LDA, PBE, and HSE results for all of the defects considered here agree to within 0.2 eV. This suggests that, when appropriate corrections are applied, the standard local and semilocal functionals can be used to screen for relevant defect configurations before using the computationally more demanding HSE functional.

ACKNOWLEDGMENTS

This work was supported by the Bundesministerium für Bildung und Forschung (03X0512G, VEKTRA), by the UCSB Solid State Lighting and Energy Center, by the National Science Foundation (NSF) (DMR-1434854), and by the Center for Low Energy Systems Technology (LEAST), one of the six SRC STARnet Centers, sponsored by MARCO and DARPA. Computational resources were provided by the Center for Scientific Computing at the CNSI and MRL (an NSF MRSEC, DMR-1121053) (NSF CNS-0960316) and by the Extreme Science and Engineering Discovery Environment (XSEDE), supported by NSF (ACI-1053575).

[1] C. G. Van de Walle and J. Neugebauer, J. Appl. Phys. **95**, 3851 (2004).
[2] S. M. Myers, A. F. Wright, M. Sanati, and S. K. Estreicher, J. Appl. Phys. **99**, 113506 (2006).
[3] C. Freysoldt, B. Grabowski, T. Hickel, J. Neugebauer, G. Kresse, A. Janotti, and C. G. Van de Walle, Rev. Mod. Phys. **86**, 253 (2014).
[4] H. Peng, D. O. Scanlon, V. Stevanovic, J. Vidal, G. W. Watson, and S. Lany, Phys. Rev. B **88**, 115201 (2013).
[5] C. Freysoldt, J. Neugebauer, and C. G. Van de Walle, Phys. Status Solidi B **248**, 1067 (2011).
[6] H.-P. Komsa, T. Rantala, and A. Pasquarello, Physica B **407**, 3063 (2012).
[7] G. Makov and M. C. Payne, Phys. Rev. B **51**, 4014 (1995).
[8] S. Lany and A. Zunger, Phys. Rev. B **78**, 235104 (2008).
[9] G. A. Baraff and M. Schlüter, Phys. Rev. B **30**, 3460 (1984).
[10] P. Bogusławski, E. L. Briggs, and J. Bernholc, Phys. Rev. B **51**, 17255 (1995).
[11] S. B. Zhang, J. Phys.: Condens. Matter **14**, R881 (2002).
[12] R. Shaltaf, G.-M. Rignanese, X. Gonze, F. Giustino, and A. Pasquarello, Phys. Rev. Lett. **100**, 186401 (2008).
[13] A. Alkauskas and A. Pasquarello, Phys. Rev. B **84**, 125206 (2011).
[14] R. Ramprasad, H. Zhu, P. Rinke, and M. Scheffler, Phys. Rev. Lett. **108**, 066404 (2012).

[15] P. G. Moses, M. Miao, Q. Yan, and C. G. Van de Walle, J. Chem. Phys. **134**, 084703 (2011).
[16] J. E. Moussa, P. A. Schultz, and J. R. Chelikowsky, J. Chem. Phys. **136**, 204117 (2012).
[17] H.-P. Komsa and A. Pasquarello, Phys. Rev. B **84**, 075207 (2011).
[18] V. Sharma, G. Pilania, G. A. Rossetti, K. Slenes, and R. Ramprasad, Phys. Rev. B **87**, 134109 (2013).
[19] D. M. Ceperley and B. J. Alder, Phys. Rev. Lett. **45**, 566 (1980).
[20] J. P. Perdew, K. Burke, and M. Ernzerhof, Phys. Rev. Lett. **77**, 3865 (1996).
[21] J. Heyd, G. E. Scuseria, and M. Ernzerhof, J. Chem. Phys. **118**, 8207 (2003).
[22] J. Heyd, G. E. Scuseria, and M. Ernzerhof, J. Chem. Phys. **124**, 219906 (2006).
[23] U. Kaufmann, P. Schlotter, H. Obloh, K. Köhler, and M. Maier, Phys. Rev. B **62**, 10867 (2000).
[24] S. Hautakangas, J. Oila, M. Alatalo, K. Saarinen, L. Liszkay, D. Seghier, and H. P. Gislason, Phys. Rev. Lett. **90**, 137402 (2003).
[25] S. M. Myers and C. H. Seager, J. Appl. Phys. **95**, 520 (2004).
[26] J. L. Lyons, A. Alkauskas, A. Janotti, and C. G. Van de Walle, Phys. Status Solidi B **252**, 900 (2015).
[27] B. Monemar, P. P. Paskov, G. Pozina, C. Hemmingsson, J. P. Bergman, S. Khromov, V. N. Izyumskaya, V. Avrutin, X. Li, H. Morkoç, H. Amano, M. Iwaya, and I. Akasaki, J. Appl. Phys. **115**, 053507 (2014).
[28] A. L. Rosa and J. Neugebauer, Phys. Rev. B **73**, 205346 (2006).
[29] N. D. M. Hine, K. Frensch, W. M. C. Foulkes, and M. W. Finnis, Phys. Rev. B **79**, 024112 (2009).
[30] C. Freysoldt, J. Neugebauer, and C. G. Van de Walle, Phys. Rev. Lett. **102**, 016402 (2009).
[31] P. E. Blöchl, Phys. Rev. B **50**, 17953 (1994).
[32] G. Kresse and J. Furthmüller, Comput. Mater. Sci. **6**, 15 (1996).
[33] G. Kresse and D. Joubert, Phys. Rev. B **59**, 1758 (1999).
[34] S. Boeck, C. Freysoldt, A. Dick, L. Ismer, and J. Neugebauer, Comp. Phys. Comm. **182**, 543 (2011).
[35] H. J. Monkhorst and J. D. Pack, Phys. Rev. B **13**, 5188 (1976).
[36] H. P. Maruska, Appl. Phys. Lett. **15**, 327 (1969).
[37] K. Laaksonen, M. G. Ganchenkova, and R. M. Nieminen, J. Phys.: Condens. Matter **21**, 015803 (2009).
[38] J. L. Lyons, A. Janotti, and C. G. Van de Walle, Phys. Rev. B **80**, 205113 (2009).
[39] A. Alkauskas, P. Broqvist, and A. Pasquarello, Phys. Status Solidi B **248**, 775 (2011).
[40] J. M. Langer and H. Heinrich, Phys. Rev. Lett. **55**, 1414 (1985).
[41] J. Coutinho, V. J. B. Torres, R. Jones, and P. R. Briddon, Phys. Rev. B **67**, 035205 (2003).
[42] M. Finnis, A. Lozovoi, and A. Alavi, Annu. Rev. Mater. Res. **35**, 167 (2005).
[43] M. Ranade, F. Tessier, A. Navrotsky, V. Leppert, S. Risbud, F. DiSalvo, and C. Balkas, J. Phys. Chem. B **104**, 4060 (2000).
[44] K. Jacob and G. Rajitha, J. Cryst. Growth **311**, 3806 (2009).
[45] T. J. Peshek, J. C. Angus, and K. Kash, J. Cryst. Growth **322**, 114 (2011).
[46] J. L. Lyons, A. Janotti, and C. G. Van de Walle, J. Appl. Phys. **115**, 012014 (2014).
[47] A. Janotti, J. B. Varley, M. Choi, and C. G. Van de Walle, Phys. Rev. B **90**, 085202 (2014).
[48] A. Janotti, J. B. Varley, P. Rinke, N. Umezawa, G. Kresse, and C. G. Van de Walle, Phys. Rev. B **81**, 085212 (2010).
[49] B. Sadigh, P. Erhart, and D. Åberg, Phys. Rev. B **92**, 075202 (2015).